Am J Cancer Res 2026;16(8):3601-3619
www.ajcr.us /ISSN:2156-6976/ajcr0171330

Original Article

Establishment an early precise diagnosis model for bone metastasis in lung cancer based on driver gene types

Sen Cao[1], Lu Bai[1], Yuehua Zhang[1], Wen Li[2], Zheng Wu[1], Xing Li[1], Jinyue Li[3], Chunwang Yang[1], Zhiyu Wang[1]

[1]Department of Immuno-Oncology, The Fourth Hospital of Hebei Medical University, Shijiazhuang, Hebei, China; [2]Department of Oncology, Hebei Medical University, Shijiazhuang, Hebei, China; [3]Department of Radiation Oncology, The Fourth Hospital of Hebei Medical University, Shijiazhuang, Hebei, China

Received January 8, 2026; Accepted August 7, 2026; Epub August 15, 2026; Published August 30, 2026

Abstract: Lung cancer has become the type of cancer with the highest incidence rate and the greatest threat of death worldwide. Bone is one of the common distant metastasis sites of lung cancer. Once a patient experiences bone metastasis, it will seriously affect the patient's quality of life and survival period. This study aimed to investigate the impact of driver gene mutations on the anatomical distribution patterns of BM in lung cancer and develop a prediction model for specific BM sites of lung cancer. From 2019 to 2023, we enrolled 353 lung cancer patients diagnosed with BM at our hospital. Associations between driver gene types and BM sites or timing were analyzed using chi-square. A predictive model was constructed through logistic regression, and its performance was evaluated using AUC, DCA, calibration curves, and independent cohort validation. The research found that driver gene types were significantly associated with the risk of simultaneous pelvic metastasis ($P < 0.001$). Logistic regression analysis identified five independent risk factors for simultaneous pelvic metastasis in lung cancer. The model demonstrated good predictive performance, with AUC values of 0.881 in the training set and 0.816 in the validation set. This study presents a novel analysis of the relationship between driver gene types and the spatio-temporal patterns of BM. Based on driver gene types, we developed an accurate nomogram model for predicting BM in lung cancer.

Keywords: Lung cancer, bone metastasis, predictive model

Introduction

Lung cancer currently exhibits the highest incidence and mortality rates among all cancer-types both in China and worldwide [1, 2]. Furthermore, according to a 30-year global assessment and projection of the economic burden of cancer, tracheal, bronchial, and lung cancers collectively account for the greatest economic cost across all cancer types [3]. Therefore, lung cancer has emerged as the world's leading cancer in terms of incidence, economic cost, and mortality. Bone tissues, particularly weight-bearing sites such as the spine, pelvis, and femur, are common sites for lung cancer metastasis. The incidence rate and disease pattern of bone metastasis vary considerably across different geographic regions [4, 5], and in some areas, bone metastasis has become the most frequent site of distant metastasis in lung cancer patients [6]. Because early-stage bone metastasis (BM) is often asymptomatic, it is frequently detected incidentally at initial staging; consequently, approximately 64.3% of lung cancer patients are diagnosed with synchronous BM at initial diagnosis, while the median time to metachronous BM is only 9 months [7]. Following the development of BM, the median survival of patients ranges from 6 to 10 months, with a 1-year survival rate of 40%-50% [8]. The occurrence of skeletal-related events (SREs), such as pathological fractures, bone pain, or spinal cord compression, further reduces median survival to only 3-5 months [8]. Furthermore, with the application of targeted therapies and immunotherapy, the survival of lung cancer patients has gradually improved, accompanied by a corresponding increase in the risk of bone

https://doi.org/10.62347/UOUD9807

metastasis. This not only severely reduces patients' quality of life and shortens their survival duration [9], but also contributes to the rising global economic burden of cancer. Therefore, early detection and diagnosis of bone metastasis, along with the implementation of individualized treatment strategies, are crucial for improving patient outcomes.

Accurate diagnosis and clinical staging are the cornerstones for effective implementation of multidisciplinary treatment (MDT), which helps prevent or delay SREs and improve patients' quality of life. Imaging examination remains the primary modality for diagnosing BM in lung cancer. Common techniques such as Emission Computed Tomography (ECT), computed tomography (CT), and magnetic resonance imaging (MRI) have significantly improved the detection of BM [10, 11]. Furthermore, the introduction of advanced imaging technologies - including PET/CT, spectral CT, and PET/MRI-has further enhanced diagnostic accuracy [12, 13]. However, the majority of patients have multiple lesions at initial presentation, with solitary metastases being relatively uncommon [14]. There are significant differences in the risk of SREs and the choice of treatment plans among different bone metastasis sites. For patients with limited BM, surgical resection is often emphasized to achieve local tumor control. In contrast, patients with widespread metastases and severe bone pain often respond poorly to local therapy alone and usually require systemic treatment, including analgesics and bone-targeting agents. However, the sensitivity of simple imaging examinations is limited, and it is extremely difficult to determine the immediate risk of SREs. Notably, approximately 50% of lung cancer patients already exhibit varying degrees of SREs at the time of initial bone metastasis diagnosis via imaging examination [15]. In addition, repeated imaging is unsuitable for frequent disease monitoring due to concerns about radiation exposure. The National Comprehensive Cancer Network (NCCN) guidelines also recommend against frequent imaging surveillance in asymptomatic patients. Therefore, current imaging modalities remain insufficient for site-specific SRE risk assessment.

Radiomics applies machine learning algorithms to extract quantitative features from medical imaging data, enabling precise characterization of tumor morphology and heterogeneity [16, 17]. The proposal and development of radiomics technology have provided new research perspectives and ideas for the precise diagnosis and treatment of tumors. The development of bone metastasis involves a complex regulatory network comprising multiple factors and pathways [18, 19]. Tumor cells undergo epithelial-mesenchymal transition (EMT) to acquire a mesenchymal-like phenotype, enabling their dissemination from the primary tumor [20]. Following invasion and extravasation, tumor cells colonize bone tissue and interact with the bone microenvironment via a range of cytokines, establishing a vicious cycle that drives bone destruction [21, 22]. This process involves multiple events associated with gene expression dysregulation and epigenetic alterations [23]. However, current radiomics-based heterogeneity assessment in lung cancer BM remains largely confined to macroscopic morphology and is thus unable to capture the underlying genetic heterogeneity or microenvironmental gene expression profiles.

Tumor-related genes are present throughout all stages of lung cancer progression, and their expression levels dynamically change in accordance with tumor initiation and development [24]. Moreover, these gene expression changes can modulate protein and metabolomic profiles, ultimately influencing clinical outcomes [20]. Multiple studies have demonstrated that patients with EGFR mutations are more likely to develop bone metastasis than those with wild-type EGFR [25-27]. Tanaka et al. further demonstrated that femoral metastasis is an independent prognostic factor in EGFR-mutant lung cancer, and that these patients have poorer responses to EGFR-TKI therapy [28]. These findings suggest that management strategies may vary by BM site, and that targeted therapy may not be optimal for all patients. A multicenter study demonstrated that patients with simultaneous bone metastasis (S-BM) have a significantly higher risk of SREs than those with metachronous bone metastasis [7]. Evidence suggests that EGFR mutation is an independent risk factor for SREs [29]. Collectively, these findings support an association between EGFR mutation and S-BM. Therefore, investigating BM distribution patterns based on genetic profiles may help address the limitations of imaging in capturing intratumoral heterogeneity and epigenetic alterations. Such an

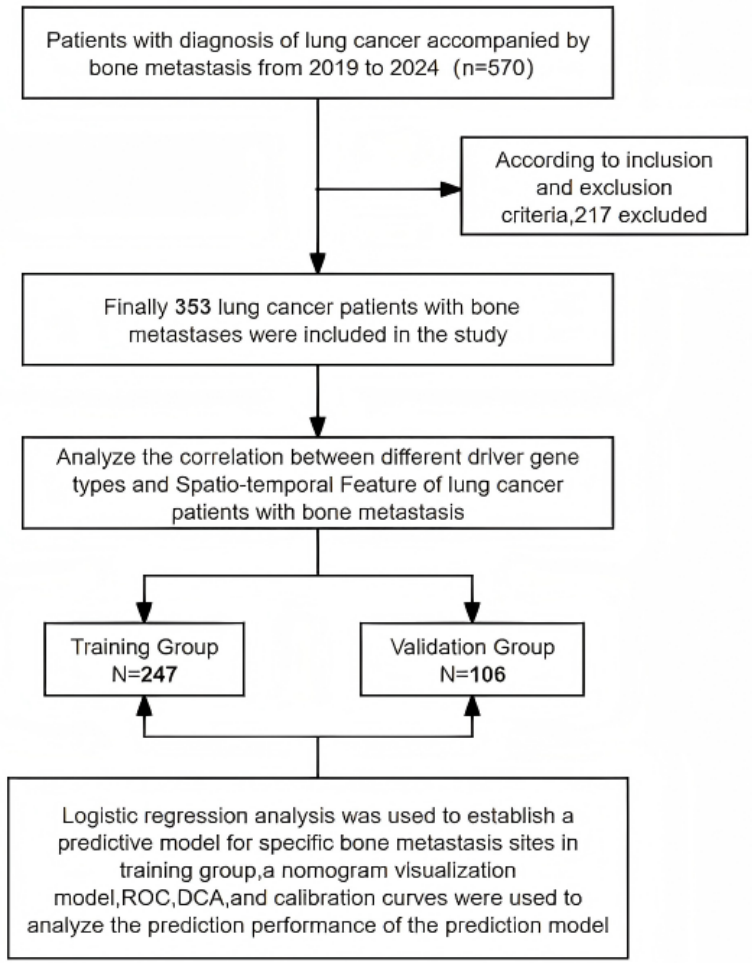

Figure 1. Flow diagram of the study. Spatial-temporal Feature: Spatial and temporal feature of bone metastasis in lung cancer patients. Spatial feature: refer to the specific anatomical sites of bone metastasis. Temporal feature: refer to the timing of bone metastasis occurrence. Bone metastasis detected within one month of lung cancer diagnosis is defined as simultaneous bone metastasis, whereas that detected beyond one month is classified as metachronous bone metastasis.

approach could significantly enhance early diagnostic accuracy and guide personalized management in BM patients.

Materials and methods

Research design

The research workflow of this study is summarized in **Figure 1**, which comprises three main phases: data screening and collection, correlation analysis between driver gene types and the spatial-temporal features of bone metastasis, and establishment and validation of a clinical prediction model. First, clinical information, imaging features of BM, and genetic sequencing results from patients with lung cancer bone metastasis were collected and statistically summarized, excluding data that did not meet the inclusion criteria. Subsequently, correlations between different driver gene types and distinct bone metastasis sites, as well as between driver gene types and the timing of bone metastasis occurrence, were analyzed. Pairwise comparisons were conducted to evaluate the influence of different driver gene types on the anatomical distribution pattern of lung cancer bone metastasis. Finally, all patients were randomly divided into a training set and a validation set at a ratio of 7:3. The prediction model was constructed in the training set and evaluated based on the area under the curve (AUC), decision curve analysis (DCA), and calibration curves. The performance of the finalized model was then assessed in the remaining 30% validation cohort.

Study subjects

All enrolled patients in this study were treated and definitively diagnosed with lung cancer and bone metastasis at the Department of Immuno-Oncology, the Fourth Hospital of Hebei Medical University, between January 2019 and December 2023. All the patients were subject to the same inclusion and exclusion criteria. The specific inclusion criteria for this study were as follows: (a) All patients were initially diagnosed with lung cancer in our hospital based on clear pathological results; (b) All enrolled patients were confirmed to have bone metastasis through imaging examinations or bone biopsy; (c) Age between 20 and 80 years; (d) All enrolled patients had clear gene sequencing results (including negative results of gene testing); (e) Complete and reliable clinical data with thorough follow-up information. The specific exclu-

sion criteria were as follows: (a) Multiple primary lung cancers or a history of other malignancies; (b) History of major bone trauma or primary bone diseases such as osteoporosis or osteoarthritis that could lead to misinterpretation of imaging findings; (c) History of endocrine disorders affecting bone metabolism, such as diabetes, thyroid disease, or parathyroid disease; and (d) Incomplete clinical data or loss to follow-up.

This study retrospectively enrolled 570 patients diagnosed with lung cancer and bone metastasis who received treatment at the Fourth Hospital of Hebei Medical University between January 2019 and December 2023. Based on the predefined inclusion and exclusion criteria, 217 patients were excluded, resulting in a final cohort of 353 patients with complete genetic profiling data. This study has been reviewed and approved by the Ethics Committee of the Fourth Hospital of Hebei Medical University (Approval No: 2025KS160). All procedures complied with the 1964 Declaration of Helsinki and the ethical principles of its subsequent amendments. Moreover, all the patients enrolled in this study underwent bone scans for screening, and PET/CT, CT, or MRI examinations, and even bone biopsies were performed on the suspected bone metastasis sites to make a clear diagnosis for different BM. Subsequently, 353 patients were randomly grouped in a 7:3 ratio into the training set (N = 247) and the validation set (N = 106) for the construction and validation of the subsequent prediction model.

Data collection

In this study, clinical information such as the general conditions of patients, laboratory examination items, pathological features, as well as the results of gene sequencing and the location, quantity, and occurrence time of bone metastases were collected by consulting the electronic medical record system, laboratory management system, and imaging examination system of our hospital. General conditions included age, gender, smoking history, and Eastern Cooperative Oncology Group (ECOG) "Score". Laboratory parameters consisted of alkaline phosphatase (ALP), lactate dehydrogenase (LDH), calcium ions (Ca^{2+}), and tumor markers such as carcinoembryonic antigen (CEA), neuron-specific enolase (NSE), cytokeratin 19 fragment antigen 21-1 (CYFRA21-1), squamous cell carcinoma antigen (SCC), pro-gastrin-releasing peptide (ProGRP), systemic inflammatory index (SII), prognostic nutritional index (PNI), and D-dimer levels. Pathological features included histological type, TNM stage, presence of peripheral or distant lymph node metastasis, and overall distant metastasis status of patients. The optimal cutoff values for SII and PNI were determined using receiver operating characteristic (ROC) curve analysis. The optimal cutoff values for the other indicators, except for the two mentioned above, were derived from the routine laboratory reference ranges of our hospital. Comprehensively consider the imaging examination results of the patient, such as bone scan, CT, MRI, PET-CT, and the pathological results of bone biopsy to clarify the specific location of bone metastasis at the first diagnosis of bone metastasis, the number of bone metastases, the type of bone metastasis, whether pathological fractures occurred, and the occurrence time of bone metastasis (simultaneous bone metastasis or metachromatic bone metastasis), etc. The composition ratio of different driver gene types is summarized in **Table 1**. EGFR mutations were the most prevalent, identified in 204 patients (57.79%). Among these, EGFR exon 19 and exon 21 mutations accounted for the majority, with 82 and 81 cases, respectively (including co-mutations of EGFR and TP53). Other driver mutations included KRAS (32 cases, 9.07%), HER2 (16 cases, 4.53%), and ALK (14 cases, 3.97%). TP53 mutations were detected in 35 patients (9.92%), though these frequently occurred as concomitant alterations. Isolated TP53 mutations were categorized into the No Driver Genes group. Other rare driver mutations, such as PIK3CA alone or co-occurring rare mutations with TP53, were classified into the Other Driver Genes group, totaling 29 cases (8.22%). For patients with incomplete clinical information, missing data were supplemented by consulting historical electronic medical records. For untested laboratory values, we applied multiple imputation (MI) to handle the missing values. Complete datasets were generated using the Multiple Imputation by Chained Equations (MICE) algorithm, and the final results were pooled using Rubin's rules to ensure the robustness and validity of our statistical inferences.

Table 1. The composition ratio of different driver gene types

Driver Gene type	N (%)	Genetic Mutations Type	N (%)
No Driver Genes	58 (16.43)	No gene mutation	50 (14.2)
		Simple TP53 mutation	8 (2.27)
EGFR	204 (57.79)	Simple EGFR 19	76 (21.53)
		Simple EGFR 21	67 (18.98)
		EGFR co-mutation	20 (5.67)
		Simple EGFR 20	11 (3.12)
		Simple EGFR 18	4 (1.13)
		Simple EGFR 17	1 (0.28)
		EGFR+TP53+	20 (5.67)
		EGFR+PIK3CA	5 (1.42)
ALK+	14 (3.97)	Simple ALK+	13 (3.68)
		ALK+RET	1 (0.28)
KRAS+	32 (9.07)	Simple KRAS	28 (7.93)
		KRAS+BRAF	2 (0.57)
		KRAS+PIK3CA	1 (0.28)
		KRAS+TP53	1 (0.28)
HER2	16 (4.53)	Simple HER2	15 (4.25)
		HER2+NRAS	1 (0.28)
Other Driver Genes	29 (8.22)	TP53 + Other Genes	6 (1.70)
		ROS1	5 (1.42)
		BRAF	6 (1.70)
		MET	4 (1.13)
		RET	4 (1.13)
		Simple PIK3CA	2 (0.57)
		NRAS	1 (0.28)
		NF1	1 (0.28)

Note: The counting data are statistically described in the form of frequency (percentage). Simple + Certain gene mutation type: The patient has only one type of gene mutation. EGFR co-mutation: Co-mutation type of the EGFR gene; Gene mutation type *a* and gene mutation type *b*: *a* represents the main driver gene, and *b* represents the concomitant gene mutation type.

Diagnostic criteria for bone metastasis: ① Patients with a confirmed pathological diagnosis of lung cancer and accompanied by typical imaging features suggestive of BM. ② Pathologically diagnosed lung cancer patients presenting with a solitary bone lesion, in whom biopsy of the bone lesion confirmed histopathological features consistent with metastatic lung cancer. The confirmation criteria for BM of lung cancer are based on either of the above two criteria.

Diagnostic criteria for S-BM: ① In this study, bone metastasis detected within one month (including one month) of lung cancer diagnosis was defined as simultaneous bone metastasis. ② Bone metastasis identified more than one month after the initial diagnosis was classified as metachronous.

Genetic testing technology: This study utilized next-generation sequencing (NGS) for genetic profiling, with specimen sources prioritized as follows: formalin-fixed paraffin-embedded (FFPE) tumor tissues - including surgical resections, bronchoscopic biopsies, CT-guided percutaneous lung biopsies, and endobronchial ultrasound-guided transbronchial needle aspirations - served as the primary source. The NGS panel used in this study was designed to detect common gene mutation types in lung cancer patients. It fully covers all the driver gene targets analyzed in this study, ensuring the accuracy and completeness of mutation detection. Cytological specimens derived from pleural or pericardial effusion, bronchial brushing/lavage fluid, or sputum were also accepted. For a minority of patients from whom neither tissue nor cytological specimens could be obtained, “liquid biopsy” was performed by detecting circulating tumor DNA (ctDNA) in peripheral blood. Due to its relatively higher technical requirements and cost, this approach was not the first-line method for initial genetic testing in the overall cohort. However, for patients with previously confirmed driver mutations, liquid biopsy was the preferred technique for monitoring the emergence of therapy-resistant mutations, thereby supporting the selection of subsequent targeted therapies.

Model derivation and validation

Statistical analysis: All statistical analyses and scientific graphing in this study were performed using SPSS 25.0, R 4.2.3, and GraphPad Prism 10.0. Continuous clinical variables were converted into categorical variables based on opti-

mal cutoff values determined by receiver operating characteristic (ROC) curve analysis. Categorical data were summarized as frequencies and percentages. Group comparisons were conducted using the chi-square test or Fisher's exact test. A logistic regression model was developed through univariate and multivariate analysis. Model performance was assessed using the AUC, DCA, and calibration curves, and was further validated in an independent validation set. A *P*-value < 0.05 was considered statistically significant.

Model construction and validation: To assess the association between driver gene types and the spatiotemporal patterns of bone metastasis, the six driver gene categories were considered as independent variables. Site-specific bone metastasis, simultaneousversus metachronous presentation, and the pattern of metastases at initial diagnosis were respectively treated as outcome variables. Group comparisons were performed using the chi-square test or Fisher's exact test. This analysis aimed to inform the subsequent development of a predictive model.

Prediction models were developed using binary logistic regression, with outcome indicators showing statistically significant differences in prior analyses serving as the dependent variables. Following hyperparameter optimization via five-fold cross-validation, the final model was retrained on the complete training set to determine feature weights and establish the fixed model structure. The resulting model was visualized as a nomogram using R software. The higher the AUC value, the stronger the discrimination of the model and the better its predictive performance. The calibration curve assesses the consistency between the predicted risk of the model and the actual observed value. The clinical practicability of the DCA curve inverse mapping model. The above indicators are used to evaluate the model in the validation queue.

Result

Analysis of the differences in Spatial-temporal Feature of BM between different driver gene types

In this study, bone metastasis sites were categorized according to anatomical structure. The spine was the most frequently involved site (249 cases, 70.54%), followed by the thoracic region (215 cases, 60.91%) and the pelvis (179 cases, 50.71%). In contrast, limb bones (113 cases, 32.01%) and the skull (51 cases, 14.45%) demonstrated relatively lower metastasis rates. Multiple BM were highly prevalent, occurring in 272 cases (77.05%), whereas solitary metastasis was observed in only 81 cases (22.95%). Regarding radiographic type, osteolytic (257 cases, 72.80%) was the most common pattern, followed by osteogenic (80 cases, 22.66%) and mixed BM (16 cases, 4.53%). Pathological fractures were identified in 44 patients (12.5%), significantly compromising their quality of life. The results of the correlation analysis between driver gene types and spatiotemporal characteristics of bone metastasis are presented in Supplementary Table 1. The incidence of pelvic metastasis varied significantly among patients with different driver gene profiles (P < 0.001). These differences remained significant after Bonferroni correction, particularly between the EGFR, HER2, and No Driver Genes groups (P < 0.001; **Figure 2A**, **2G**). Further analysis of metastatic patterns across EGFR subtypes (Supplementary Table 2) revealed a significant difference in the incidence of spinal metastasis within the overall EGFR-mutant population (P = 0.042), though post-hoc pairwise comparisons did not identify significant intergroup differences (**Figure 2D**). Simultaneous bone metastasis was considerably more frequent than metachronous metastasis across all driver gene types and EGFR subtypes. This difference reached statistical significance among different driver gene categories (P = 0.006), but not within EGFR subtypes (**Figure 2B**, **2E**).

Further analysis of bone metastasis patterns at the initial diagnosis of lung cancer revealed statistically significant differences in the incidence of simultaneous pelvic metastasis (P < 0.001) and simultaneous spinal metastasis (P = 0.033) among patients stratified by driver gene types and EGFR classifications. Consistent with the aforementioned findings, driver gene-positive patients demonstrated significantly higher rates of simultaneous pelvic metastasis compared to driver gene-negative patients (P < 0.001). Post-hoc analysis confirmed particularly prominent differences between the EGFR and HER2 mutation groups relative to the No Driver Genes group (**Figure**

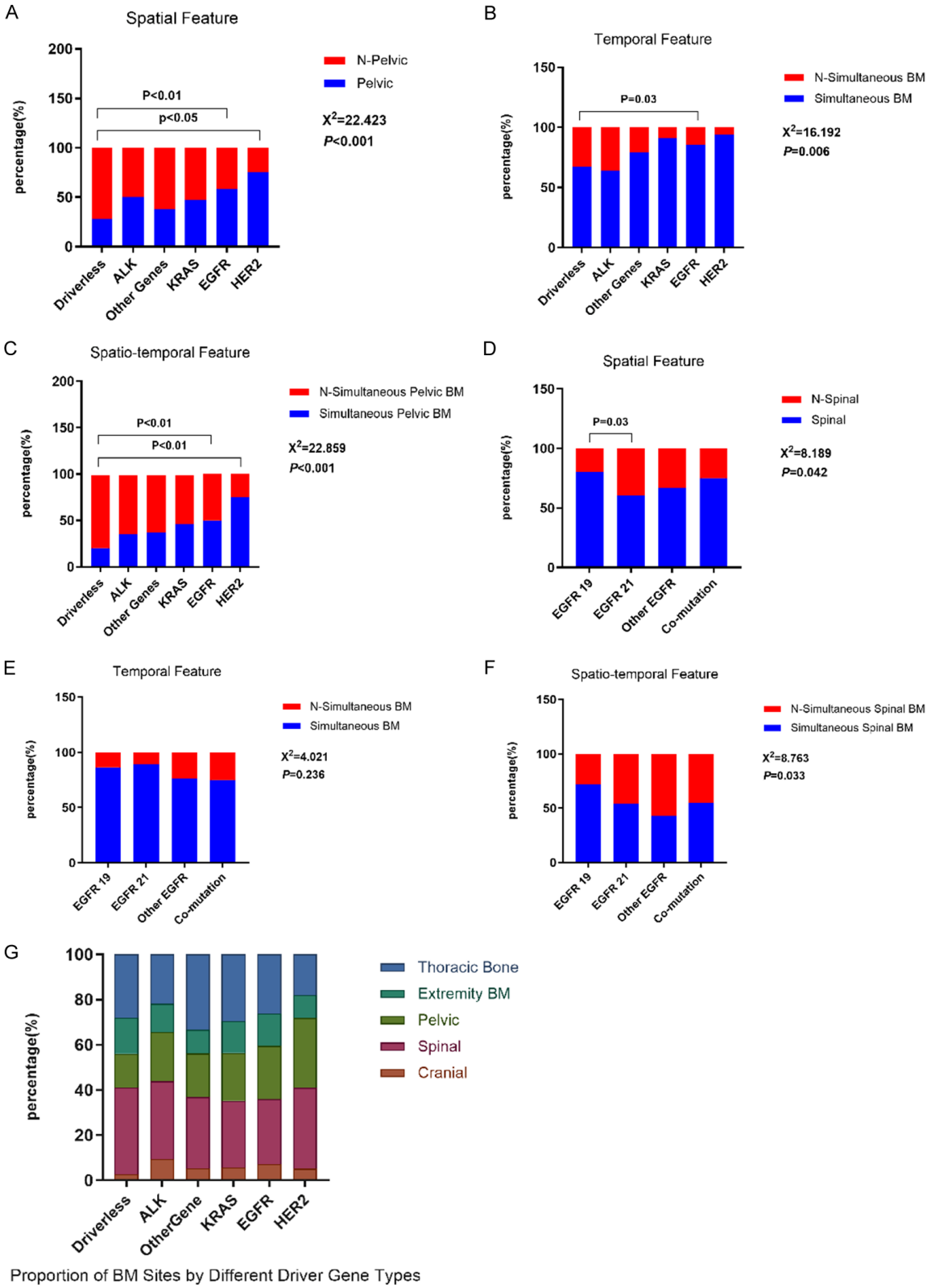

Figure 2. Analysis of the association between driver gene types and the spatial-temporal feature of bone metastasis. (A-C) Present the comparative analyses of different driver gene types with spatial, temporal, and integrated spatiotemporal patterns of lung cancer bone metastasis, respectively. In the spatial (A) and spatiotemporal (C) analyses, pelvic metastasis demonstrated a statistically significant association with driver gene status ($P < 0.001$),

while no significant differences were observed at other metastatic sites. (D-F) Show the corresponding analyses of spatial, temporal, and spatiotemporal characteristics according to EGFR mutation subtypes within the EGFR-mutant population. In the spatial (D) and spatiotemporal (F) assessments, spinal metastasis exhibited statistically significant variation across EGFR subtypes ($P < 0.05$), with no significant differences detected at other metastatic locations. (G) Illustrates the distribution of bone metastasis sites stratified of the entire study cohort by different driver gene types. Abbreviations: BM: bone metastasis. Pelvic/N-Pelvic: represent patients with pelvic metastasis and those without pelvic metastasis. Spinal/N-Spinal: represent patients with Spinal metastasis and those without Spinal metastasis. N-simultaneous: without simultaneous bone metastasis/metachronous bone metastasis.

2C, **2F**). However, no statistically significant variations were observed among different EGFR subtypes regarding simultaneouspelvic or spinal metastases. Additionally, comparative analysis between EGFR/TP53 co-mutation and EGFR/TP53 wild-type subgroups showed no significant differences in metastatic sites or timing of bone metastasis onset. Further investigation revealed no statistically significant associations between driver gene types and the number of BM, radiographic type of bone lesions, or incidence of pathological fractures ($P > 0.05$).

Patient characteristics

As demonstrated in the preceding analyses, there are significant differences in "simultaneous pelvic metastasis" among different types of driver genes. Driver gene-positive patients exhibited a higher propensity for pelvic metastasis compared to their driver gene-negative counterparts, with the HER2 and EGFR mutation groups showing the highest incidence rates. Although statistical significance was observed in simultaneous spinal metastasis across EGFR subtypes overall, post-hoc pairwise comparisons revealed no significant intergroup differences. These findings support the selection of simultaneous pelvic metastasis as the primary outcome indicator for subsequent predictive modeling. The 353 eligible patients were randomly allocated into a training set (N = 247) and a validation set (N = 106) at a 7:3 ratio. The two groups demonstrated comparable baseline characteristics, including age, gender, pathological type, TNM stage, driver gene profiles, and distribution of bone metastasis sites, with no statistically significant differences ($P > 0.05$; see Supplementary Table 3). Within the training set, 111 patients presented with simultaneous pelvic metastasis at initial lung cancer diagnosis, while 136 patients showed no radiological evidence of pelvic involvement at diagnosis. Among the latter group, some developed metachronous pelvic metastasis during follow-up, while others remained free of pelvic metastasis until death or the end of the study period.

Variable selection

Univariate logistic regression analysis of factors influencing S-pelvic metastasis in lung cancer patients: The clinical data of the patients were included in the logistic regression model for univariate analysis. The results indicated that the following factors demonstrated no statistically significant associations: age, gender, smoking history, ECOG score, Ca^{2+}, SCC, CYFRA21-1, SII, PNI, T stage, N stage, number of lung cancer lesions, regional lymph node metastasis, distant lymph node metastasis, and distant metastasis. In contrast, thirteen variables showed statistically significant differences: ALP ($P < 0.001$), LDH ($P = 0.007$), ProGRP ($P < 0.001$), CEA ($P = 0.034$), NSE ($P = 0.039$), D-dimer ($P = 0.036$), pathological type ($P = 0.014$), driver gene type ($P < 0.001$), number of BM ($P < 0.001$), S-Cranial BM ($P < 0.001$), S-Spinal BM ($P < 0.0001$), S-Extremity BM ($P < 0.0001$), and S-Thoracic BM ($P < 0.0001$). Detailed results are presented in **Table 2**. Multicollinearity analysis of these 13 significant variables revealed that all variance inflation factor (VIF) values were below 2, indicating no substantial multicollinearity among the predictors.

Multivariate logistic regression analysis of factors influencing S-pelvic metastasis in patients with lung cancer: Variables showing statistical significance in the univariate analysis were subsequently included in a multivariable logistic regression model (**Table 3**). The results identified the following independent risk factors for simultaneouspelvic metastasis in lung cancer patients: ProGRP > 69.2 pg/mL ($P = 0.011$), driver gene type ($P = 0.006$), multiple BM ($P = 0.001$), S-Spinal BM ($P = 0.002$), and S-Extremity BM ($P = 0.001$), as visualized in **Figure 3**. The remaining eight variables did not

Table 2. Comparison of clinical data between simultaneous pelvic BM group and Metachronous pelvic BM group

Factors	Simultaneous Pelvic Metastasis		χ^2	*P*
	Yes N = 111 (%)	*No* N = 136 (%)		
Age			1.947	0.163
< 60	48 (43.2)	47 (34.6)		
≥ 60	63 (56.8)	89 (65.4)		
Gender			3.187	0.074
Male	51 (45.9)	78 (57.4)		
Female	60 (54.1)	58 (42.6)		
Smoking history			1.806	0.405
Never	76 (68.5)	82 (60.3)		
Past	22 (19.8)	35 (25.7)		
Current	13 (11.7)	19 (14.0)		
ECOG			1.670	0.196
0-2	57 (51.4)	81 (59.6)		
> 2	54 (48.6)	55 (40.4)		
ALP (U/L)			16.367	P < 0.001
≤ 150	71 (64.0)	117 (86.0)		
> 150	40 (36.0)	19 (14.0)		
LDH (U/L)			7.345	0.007
≤ 250	58 (52.3)	94 (69.1)		
> 250	53 (47.7)	42 (30.9)		
Ca^{2+} (mmol/L)			0.103	0.749
≤ 2.52	107 (96.4)	130 (95.6)		
> 2.52	4 (3.6)	6 (4.4)		
ProGRP (pg/ml)			12.140	P < 0.001
≤ 69.2	76 (68.5)	118 (86.8)		
> 69.2	35 (31.5)	18 (13.2)		
SCC (ng/L)			1.870	0.171
≤ 2.7	99 (89.2)	113 (83.1)		
> 2.7	12 (10.8)	23 (16.9)		
CEA (ng/L)			4.513	0.034
≤ 5	17 (15.3)	36 (26.5)		
> 5	94 (84.7)	100 (73.5)		
CYFRA21-1 (ng/L)			3.225	0.073
≤ 3.3	14 (12.6)	29 (21.3)		
> 3.3	97 (87.4)	107 (78.7)		
NSE (ng/L)			4.280	0.039
≤ 16.5	37 (33.3)	63 (46.3)		
> 16.5	74 (66.7)	73 (53.7)		
SII			0.368	0.544
≤ 609.9	28 (25.2)	39 (28.7)		
> 609.9	83 (74.8)	97 (71.3)		
PNI			1.522	0.217
≤ 45.75	38 (34.2)	57 (41.9)		
> 45.75	73 (65.8)	79 (58.1)		
D-dimer (mg/L)			4.383	0.036
< 0.243	33 (29.7)	58 (42.6)		
≥ 0.243	78 (70.3)	78 (57.4)		

Pathological type			8.601	0.014
Squamous Cell Carcinoma	1 (0.9)	13 (9.5)		
Adenocarcinoma	105 (94.6)	118 (86.8)		
Other type	5 (4.5)	5 (3.7)		
T stage			3.096	0.078
T1-T2	36 (32.4)	59 (43.4)		
T3-T4	75 (67.6)	77 (56.6)		
N stage			3.431	0.064
N0-N1	22 (19.8)	41 (30.1)		
N2-N3	89 (80.2)	95 (69.9)		
Number of lung cancer lesions			0.080	0.778
Single	84 (75.7)	105 (77.2)		
Multiple	27 (24.3)	31 (22.8)		
Regional lymph node metastasis			0.072	0.789
No	16 (14.4)	18 (13.2)		
Yes	95 (85.6)	118 (86.8)		
Distant lymph node metastasis			0.601	0.438
No	50 (45.0)	68 (50.0)		
Yes	61 (55.0)	68 (50.0)		
Distant metastasis			1.257	0.262
No	16 (85.6)	27 (19.9)		
Yes	95 (14.4)	109 (80.1)		
Driver Gene type			24.726	P < 0.001
Driverless Mutation	8 (7.2)	36 (26.5)		
ALK+	3 (2.7)	7 (5.1)		
Other Driver Genes	8 (7.2)	13 (9.6)		
KRAS+	10 (9.0)	11 (8.1)		
EGFR+	71 (64.0)	67 (49.3)		
HER2+	11 (9.9)	2 (1.5)		
Number of BM			40.340	P < 0.001
Single	6 (5.4)	55 (40.4)		
Multiple	105 (94.6)	81 (59.6)		
S-Cranial BM			15.114	P < 0.001
No	87 (78.4)	129 (94.9)		
Yes	24 (21.6)	7 (5.1)		
S-Spinal BM			53.551	P < 0.0001
No	21 (18.9)	89 (65.4)		
Yes	90 (81.1)	47 (34.6)		
S-Extremity BM			47.754	P < 0.0001
No	58 (52.3)	124 (91.2)		
Yes	53 (47.7)	12 (8.8)		
S-Thoracic BM			23.199	P < 0.0001
No	36 (32.4)	86 (63.2)		
Yes	75 (67.6)	50 (36.8)		

Note: ECOG: Eastern Cancer Collaboration Physical Condition Scale; SII: Systemic Inflammation Index; PNI: Prognostic Nutritional Index; S-pelvic BM: Simultaneous pelvic metastasis; S-Cranial BM: Simultaneous cranial metastasis; S-Spinal BM: Simultaneous spinal metastasis; S-Extremity BM: Simultaneous limb bone metastasis; S-Thoracic BM: Simultaneous bone metastasis in the thoracic group.

Table 3. Multifactor logistic regression analysis of factors influencing simultaneous pelvic metastasis in lung cancer

Factors	β	SE	Ward (χ^2)	P	OR	95% CI	
						Lower limit	Upper limit
ALP	0.333	0.455	0.535	0.465	1.395	0.572	3.405
LDH	0.392	0.402	0.949	0.330	1.48	0.673	3.253
ProGRP	1.305	0.510	6.537	0.011*	3.688	1.356	10.03
CEA	0.842	0.522	2.595	0.107	2.320	0.833	6.460
NSE	0.292	0.381	0.588	0.443	1.339	0.635	2.827
D-dimer	0.324	0.400	0.654	0.419	1.383	0.631	3.031
Pathological type			0.213	0.899			
Adenocarcinoma	0.014	1.226	< 0.001	0.991	1.014	0.092	11.212
Other type	0.582	1.695	0.118	0.731	1.789	0.065	49.566
Driver Gene type			16.450	0.006*			
ALK	1.519	1.094	1.928	0.165	4.566	0.535	38.958
Other Driver Genes	1.302	0.819	2.530	0.112	3.677	0.739	18.292
KRAS	1.819	0.832	4.786	0.029	6.168	1.209	31.476
EGFR	1.705	0.617	7.625	0.006	5.502	1.640	18.454
HER2	4.867	1.252	15.117	< 0.001	129.914	11.173	1510.622
Number of BM	1.860	0.568	10.700	0.001*	6.421	2.107	19.566
S-Cranial BM	0.600	0.644	0.868	0.352	1.822	0.516	6.436
S-Spinal BM	1.221	0.396	9.504	0.002*	3.391	1.560	7.369
S-Extremity BM	1.744	0.503	12.045	0.001*	5.720	2.136	15.317
S-Thoracic BM	0.141	0.410	0.119	0.730	1.152	0.516	2.570

Note: *There is a statistically significant difference. Number of BM: Number of BM; S-Cranial BM: Simultaneous cranial metastasis; S-Spinal BM: Simultaneous spinal metastasis; S-Extremity BM: Simultaneous Extremity metastasis; S-Thoracic BM: Simultaneous bone metastasis in the thoracic group; Lower limit: Lower limit of the 95% confidence interval; upper limit: The upper limit of the 95% confidence interval.

retain statistical significance in the multivariable analysis (P > 0.05).

Development and evaluation of the S-Pelvic metastasis diagnostic model

A total of 5 independent risk factors for simultaneous pelvic metastasis were screened out through Logistics regression analyses. In our Training Group (N = 247), there were a total of 111 positive events. According to the "Events Per Variable (EPV)" principle, EPV > 22. This indicates that our sample size is sufficient to support the 5 independent predictors included in the final multivariate model. We incorporated these five variables into R software to construct a visual nomogram prediction model (**Figure 4**). Different ProGRP values, Driver Gene types, Number of BM, S-Spinal BM, and S-Extremity BM correspond to different scores respectively. The total score obtained by adding each score can be used to obtain the corresponding prediction probability. For example, ProGRP values ≤ 69.2, Spinal Metastasis "No", Limbs Extremities "No", Number of Bone Metastasis "Multiple", Driver gene type "Driver gene type". The total score for this patient is 75, corresponding to a risk probability of 0.193 (Supplementary Table 4). The model demonstrated excellent discriminative ability for predicting simultaneous pelvic metastasis, with AUC of 0.881 in the training set (**Figure 5A**). This robust performance was maintained in the validation set, where the AUC reached 0.816 (**Figure 5B**), indicating consistently strong predictive accuracy and high diagnostic value. Calibration curves revealed close agreement between model predictions and observed outcomes in both training and validation cohorts (**Figure 5C** and **5D**). The DCA curve is an effective method for evaluating the clinical benefit degree of disease diagnosis models. The DCA curves shown in **Figure 5E** and **5F** further confirm that this model has a very high clinical net benefit. Additionally, to evaluate the discriminative performance of the predictive model across different mutation groups, we conducted subgroup analyses for various driver

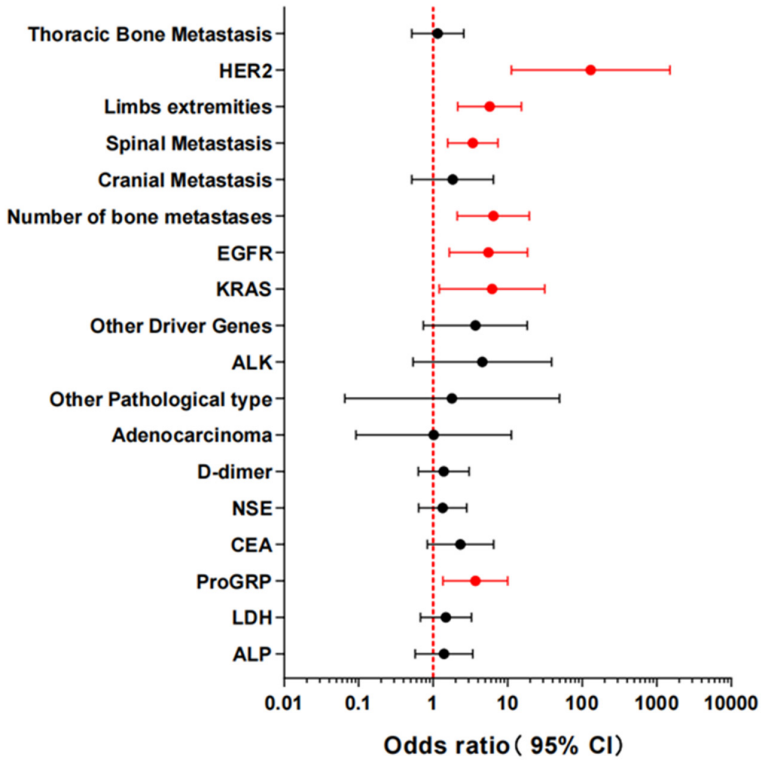

Figure 3. Multivariate logistic regression analysis.

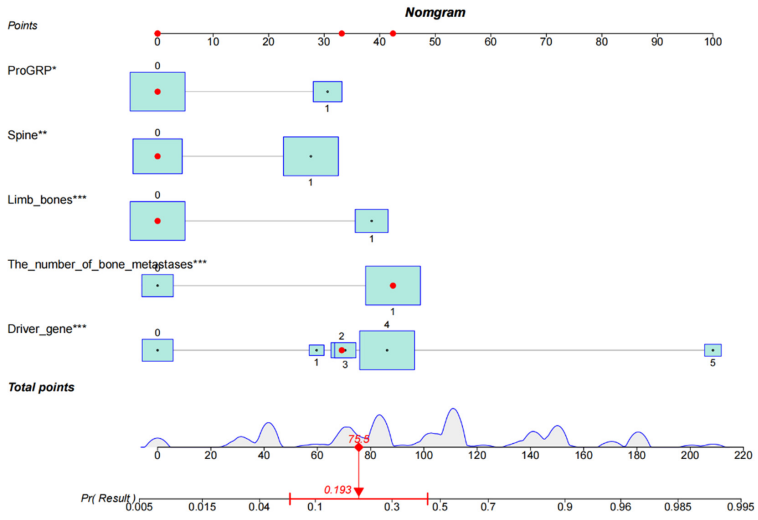

Figure 4. Nomogram model predicting simultaneous pelvic metastasis in lung cancer patients.

genes, and generated ROC curves and evaluation tables. The ALK mutation group exhibited the optimal AUC value and highest accuracy (**Table 4**). Furthermore, this model demonstrated excellent discriminative power and accuracy across other driver gene subgroups (Supplementary Figure 1).

Discussion

Lung cancer incidence and mortality rates have been rising annually, surpassing breast cancer to become the malignancy with the highest global risk. Concurrently, lung cancer imposes the heaviest economic burden and poses the greatest threat of mortality worldwide [1-3]. The incidence of bone metastasis in lung cancer patients ranges from 30% to 40% [30]. Approximately 30% to 70% of patients with BM develop skeletal-related events (SREs) of varying severity [15]. A small number of patients may even experience it multiple times, seriously affecting their quality of life. Current imaging modalities remain significantly limited. Feature extraction is generally confined to epiphenomenal morphological characteristics, lacking deeper exploration of intrinsic genetic patterns. Moreover, the patient's subjective will still holds the dominant position, and imaging examinations are often considered only when obvious symptoms appear. At this point, the patient has already missed the golden treatment period, and the risk of developing SREs has greatly increased [31]. There is no unified standard for the selection sequence of systemic and local treatment for bone metastasis of lung cancer, and the treatment methods lack specificity, resulting in some patients missing the best treatment opportunity. With the increasing maturation of the multidisciplinary team (MDT) model, both domestic and international guidelines emphasize the importance of collaborative expert discussion, continuous assessment based on disease progression, and the development of personalized treatment strategies. Consequently, there is an

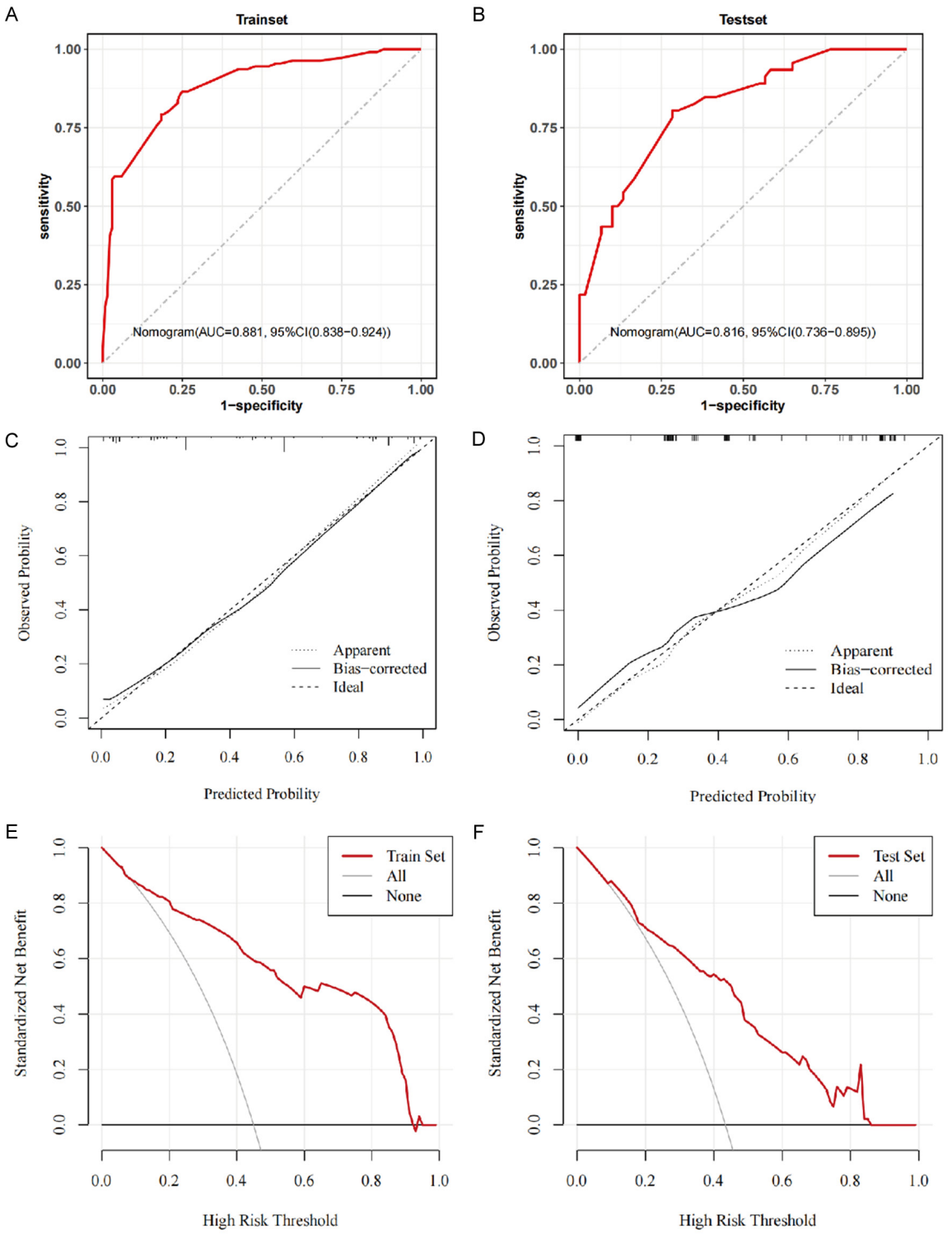

Figure 5. Performance evaluation of the nomogram prediction model in the training group and validation group. (A) and (B) are the ROC curves of the model in the training cohort and validation cohort of the nomogram prediction model, respectively; (C) and (D) are respectively the calibration curves of the nomogram prediction model in the training queue and the validation queue; (E) and (F) are respectively the DCA curves of this model in the training queue and the validation queue; ROC: Receiver Operating Characteristic curve; AUC: Area under the curve; DCA: Clinical Decision Curve Analysis.

Table 4. Evaluation table for subgroup analyses of different driver genes

Group	AUC	Accuracy	PPV	NPV	Precision	Recall	F1
Driverless Mutation	0.885	0.886	0.667	0.943	0.667	0.750	0.706
ALK+	0.976	0.900	0.750	1.000	0.750	1.000	0.857
Other Driver Genes	0.803	0.810	1.000	0.765	1.000	0.500	0.667
KRAS+	0.873	0.857	0.889	0.833	0.889	0.800	0.842
EGFR+	0.854	0.768	0.953	0.684	0.953	0.577	0.719
HER2+	0.773	0.538	1.000	0.250	1.000	0.455	0.625

Note: ROC: Receiver Operating Characteristic curve; AUC: Area under the Receiver Operating Characteristic curve; PPV: Positive Predictive Value; NPV: Negative Predictive Value.

urgent need to establish a simple, non-invasive, and efficient diagnostic tool that can identify optimal treatment approaches for patients with varying risks of bone metastasis, aiming to prevent or delay the onset and progression of SREs. This study links the types of gene mutations with the spatiotemporal specificity of bone metastasis, preliminarily explores the anatomical distribution pattern of bone metastasis in lung cancer, and reveals the intrinsic genetic laws of patients. We attempt to early predict the risk of site-specific bone metastasis by integrating gene mutation profiles with routine clinical data, thereby enabling "tailor-made" personalized treatment strategies based on individual metastasis patterns to improve quality of life and prolong survival.

The findings of this study demonstrate that the spine is the most frequent site of bone metastasis in lung cancer, followed by the ribs, pelvis, sternum, and femur, while the humerus, distal limbs, and clavicle are least commonly involved. This pattern suggests that lung cancer cells preferentially metastasize to well-vascularized axial skeletal sites and bones adjacent to the primary tumor, consistent with current literature [32, 33]. In our study, the driver gene mutation rate of NSCLC patients with bone metastasis reached 87.81% (320 cases), significantly higher than that reported in NSCLC patients without confirmed bone metastasis [34]. EGFR mutations remained the most prevalent alteration (61.56%) in this subgroup [35]. Our definition of simultaneous bone metastasis is based on standard clinical research practices, emphasizing bone metastatic events detected within a specific time window. Our study observed a significantly higher prevalence of multiple bone metastases compared to solitary metastases, this is consistent with the findings of most current studies [7, 36]. This disparity is significantly associated with regional limitations, differences in study populations, and variations in detection modalities. Specifically, our study utilized high-resolution imaging techniques such as PET-CT and MRI, which may be more sensitive in detecting small or occult bone lesions, thereby leading to a higher detection rate of multiple bone metastases. Furthermore, the pelvis comprises diverse bones and complex anatomical structures with abundant vascular and lymphatic networks. This makes it a high-risk area for hematogenous metastasis of lung cancer cells, where cancer cells are prone to forming multifocal metastases [37, 38]. This discrepancy also highlights a limitation of our study as a single-center retrospective analysis. Further analysis revealed significant differences in pelvic metastasis risk across the six driver gene types. Specifically, patients with EGFR and HER2 mutations exhibited the highest incidence of pelvic metastasis, showing statistically significant differences compared to those in the no-driver-gene group ($P < 0.05$). This suggests that EGFR and HER2 mutations may influence tumor cell behavior within the bone microenvironment and enhance metastatic potential to pelvic sites. We developed an innovative nomogram prediction model based on driver gene types for early precise diagnosis and risk stratification of lung cancer patients with BM. The model demonstrated strong predictive performance, with AUC values of 0.881 and 0.816 in the training set and validation set respectively. Evaluation using calibration curves and DCA confirmed excellent model stability and clinical utility. These results indicate that driver gene status may serve as a precise predictor for bone metastasis patterns, providing guidance for targeted drug development in this patient population Therefore, this model can provide early diagnosis and treatment value for patients

initially diagnosed with lung cancer accompanied by bone metastasis, but it is not yet clear whether pelvic metastasis has occurred, avoiding the need for hip MRI, PET/CT and other examinations at the initial diagnosis. Moreover, it addresses challenges in treatment response assessment caused by uncertain pelvic metastasis status, thereby informing subsequent treatment selection. Given that sacral involvement carries risk of spinal cord compression, and pelvic metastases-particularly in weight-bearing regions like the acetabulum-significantly impair mobility and quality of life, early detection and preventive intervention are crucial for optimizing clinical management of lung cancer patients with bone metastasis.

Consistent with existing literature [14], the majority of bone metastatic lesions in this study presented as multiple involvement, with solitary metastasis observed only in a small subset of patients at initial assessment. In this study, we observed that patients in the synchronous pelvic metastasis subgroup had a higher risk of developing spinal metastases compared to the overall study cohort. This suggests a stronger co-occurrence between pelvic and spinal metastases. Both the spine and the pelvis possess complex skeletal architectures and are richly supplied with red marrow, as well as extensive vascular and neural networks. These characteristics facilitate tumor cell adhesion and colonization. This is also closely associated with the anatomical proximity between the two sites. Both EGFR and HER2 belong to the epidermal growth factor receptor family and are frequently high expressed in lung cancer tissues, where they collaboratively facilitate cell invasion and metastatic. Relevant studies have shown that tumor cells with gene mutations exhibit stronger invasive characteristics and distant metastasis ability than those without gene mutations, especially in terms of brain metastasis and bone metastasis [39, 40]. This may be related to its proliferative characteristics. Tumor cells with EGFR and HER2 mutations have a selective proliferative advantage over non-mutated cells in their growth state. Even under conditions of nutrient deficiency, they can still maintain their proliferative potential, helping tumor cells to metastasize to bones, skulls and other parts through the bloodstream [41]. Meanwhile, exosomes derived from non-small cell lung cancer (NSCLC) have been shown to activate EGFR signaling through secretion of amphiregulin (AREG) [27]. EGFR pathway activation further interacts with bone microenvironment cytokines to upregulate RANKL (receptor activator of nuclear factor kappa-B ligand) expression, indirectly promoting osteoclastogenesis [42, 43] and thereby facilitating bone invasion and colonization by lung cancer cells. Although multiple studies confirm significantly higher bone metastasis incidence in EGFR-mutated versus wild-type lung cancer patient [25, 27, 44], direct evidence linking EGFR expression specifically to pelvic metastasis remains elusive [42]. This association warrants further investigation to elucidate the underlying molecular mechanisms and clinical implications. Research on HER2 mutations is currently mainly focused on breast cancer and prostate cancer, with less involvement in lung cancer-related studies. HER2 expression status constitutes an independent risk factor for bone metastasis in breast cancer [45]. And activation of HER2 signaling enhances circulating tumor cell survival and supports bone tropism in prostate cancer [46]. Alterations in HER2 not only contribute to the abnormal proliferation and survival of tumor cells but also promote angiogenesis, mesenchymal characteristics, and tumor immune evasion [47]. This mechanism endows HER2-mutated tumor cells with a stronger propensity for pelvic invasion. With the involvement of various cytokines, these cells can successfully colonize the pelvis through interactions with the bone microenvironment. Further research and exploration are warranted in the future.

This study revealed the correlation between driver gene mutations and the spatiotemporal specificity of bone metastasis within patients with lung cancer bone metastasis for the first time, enhancing everyone's understanding and recognition of the anatomical patterns of lung cancer bone metastasis. Furthermore, we developed a concise and efficient predictive model for simultaneouspelvic metastasis, which may facilitate improved clinical management of pelvic metastatic disease. However, this study also has some limitations. Although rare mutations such as HER2 and ALK mutations exhibit substantial effect sizes with OR significantly greater than 1, the wide confidence intervals cannot obscure the inherent limitations of this

study. Among the training group samples, the incidence of simultaneous pelvic metastasis in the HER2 mutation group reached as high as 84.62% (11/13), which is significantly higher than that observed in other mutation types, suggesting that HER2 mutations carry a higher risk ratio for pelvic metastasis in early-stage lung cancer. Additionally, due to the low incidence of HER2 mutations and the relatively small sample size, resulting in an extremely high odds ratio of 129.914. We will continue to collect such samples from larger cohorts, with the aim of obtaining more stable odds ratios across broader datasets. Bone metastases lesions in early-stage lung cancer are often difficult to detect, due to economic constraints, some patients do not undergo NGS, and patients have a short survival duration, making follow-up data collection challenging; making it hard to obtain a sufficiently large sample size, which consequently imposes certain limitations on the model's extrapolation capabilities. In future studies, we will continue to collect such samples, expand our database, and systematically collect patients' survival data; subsequently, we will conduct joint predictive analyses and subsequent extrapolation of results based on this model using larger sample sizes. Due to the presence of intratumoral genetic heterogeneity and variations in tissue sampling, NGS detection results exhibit heterogeneity. Additionally, most NGS testing were restricted to some common lung cancer-associated genes, which may affect the generalizability of the findings. In the future, we will constantly improve the model to obtain more convincing research results.

Conclusion

This study explored for the first time the intrinsic genetic laws and anatomical distribution models of bone metastasis from lung cancer. By integrating driver gene types with clinicopathological characteristics, we developed a predictive model for simultaneous pelvic metastasis in lung cancer patients. The model demonstrated high predictive accuracy for pelvic metastasis at initial lung cancer diagnosis and was effectively visualized using a nomogram. This model provides a powerful tool for the early precise diagnosis and personalized treatment of patients with bone metastasis from lung cancer. It is helpful for everyone to understand that bone metastasis is not merely a single metastatic site. We need to more precisely distinguish the intrinsic characteristics of different bone metastasis sites, thereby strengthening the clinical management of patients with bone metastasis and preventing or delaying the occurrence of SREs.

Acknowledgements

We thank all the researchers in the Oncology Immunology Laboratory. This work was supported in part by Natural Science Foundation of Hebei Province, Grant Numbers: H2024-206210 and Central Guidance for Local Science and Technology Development Fund Project, Grant Numbers: 226Z7717G.

Disclosure of conflict of interest

None.

Address correspondence to: Zhiyu Wang, Department of Immuno-Oncology, The Fourth Hospital of Hebei Medical University, No. 12 Jiankang Road, Shijiazhuang 050000, Hebei, China. E-mail: drwangzhiyu@hebmu.edu.cn

References

[1] Global cancer burden growing, amidst mounting need for services. Saudi Med J 2024; 45: 326-327.

[2] Zheng RS, Chen R, Han BF, Wang SM, Li L, Sun KX, Zeng HM, Wei WW and He J. Cancer incidence and mortality in China, 2022. Zhonghua Zhong Liu Za Zhi 2024; 46: 221-231.

[3] Chen S, Cao Z, Prettner K, Kuhn M, Yang J, Jiao L, Wang Z, Li W, Geldsetzer P, Bärnighausen T, Bloom DE and Wang C. Estimates and projections of the global economic cost of 29 cancers in 204 countries and territories from 2020 to 2050. JAMA Oncol 2023; 9: 465-472.

[4] Hernandez RK, Wade SW, Reich A, Pirolli M, Liede A and Lyman GH. Incidence of bone metastases in patients with solid tumors: analysis of oncology electronic medical records in the United States. BMC Cancer 2018; 18: 44.

[5] Phanphaisarn A, Patumanond J, Settakorn J, Chaiyawat P, Klangjorhor J and Pruksakorn D. Prevalence and survival patterns of patients with bone metastasis from common cancers in Thailand. Asian Pac J Cancer Prev 2016; 17: 4335-4340.

[6] Wang X, Wang Z, Pan J, Lu ZY, Xu D, Zhang HJ, Wang SH, Huang DY and Chen XF. Patterns of extrathoracic metastases in different histologi-

cal types of lung cancer. Front Oncol 2020; 10: 715.
[7] Hong S, Youk T, Lee SJ, Kim KM and Vajdic CM. Bone metastasis and skeletal-related events in patients with solid cancer: a Korean nationwide health insurance database study. PLoS One 2020; 15: e0234927.
[8] Wu S, Pan Y, Mao Y, Chen Y and He Y. Current progress and mechanisms of bone metastasis in lung cancer: a narrative review. Transl Lung Cancer Res 2021; 10: 439-451.
[9] Dong H, Lan A, Gao J, An Y, Chu L, Yang X, Chu X, Hu J, Chu Q, Ni J and Zhu Z. Prognostic significance of bone metastasis and clinical value of bone radiotherapy in metastatic non-small cell lung cancer receiving PD-1/PD-L1 inhibitors: results from a multicenter, prospective, observational study. Transl Lung Cancer Res 2024; 13: 2603-2616.
[10] Lin L, Zheng R, Geng J, Wang X, Li M, Fan R, Zheng Y and Yang K. Skeletal standardized uptake values obtained using quantitative SPECT/CT for the detection of bone metastases in patients with lung adenocarcinoma. Front Med (Lausanne) 2023; 10: 1119214.
[11] Stecco A, Trisoglio A, Soligo E, Berardo S, Sukhovei L and Carriero A. Whole-body MRI with diffusion-weighted imaging in bone metastases: a narrative review. Diagnostics (Basel) 2018; 8: 45.
[12] Luo H, Zou L, Yang Q, Yuan C, Ma K, Yang S, Luo D, Liu C and Liu Z. Spectral CT assists differentiation of osteoblastic bone metastasis from bone island in newly diagnosed cancer patients. Eur Radiol 2024; 34: 60-68.
[13] Li EC and Davis LE. Zoledronic acid: a new parenteral bisphosphonate. Clin Ther 2003; 25: 2669-2708.
[14] Ettinger DS, Wood DE, Akerley W, Bazhenova LA, Borghaei H, Camidge DR, Cheney RT, Chirieac LR, D'Amico TA, Demmy TL, Dilling TJ, Dobelbower MC, Govindan R, Grannis FW Jr, Horn L, Jahan TM, Komaki R, Krug LM, Lackner RP, Lanuti M, Lilenbaum R, Lin J, Loo BW Jr, Martins R, Otterson GA, Patel JD, Pisters KM, Reckamp K, Riely GJ, Rohren E, Schild SE, Shapiro TA, Swanson SJ, Tauer K, Yang SC, Gregory K and Hughes M; National comprehensive cancer network. Non-small cell lung cancer, version 6.2015. J Natl Compr Canc Netw 2015; 13: 515-524.
[15] Ulas A, Bilici A, Durnali A, Tokluoglu S, Akinci S, Silay K, Oksuzoglu B and Alkis N. Risk factors for skeletal-related events (SREs) and factors affecting SRE-free survival for nonsmall cell lung cancer patients with bone metastases. Tumour Biol 2016; 37: 1131-1140.
[16] Qi C, Wang C, Zhao L, Zhu Z, Wang P, Zhang S, Cheng L and Zhang X. SCovid: single-cell atlases for exposing molecular characteristics of COVID-19 across 10 human tissues. Nucleic Acids Res 2022; 50: D867-D874.
[17] Tavolara TE, Gurcan MN, Segal S and Niazi MKK. Identification of difficult to intubate patients from frontal face images using an ensemble of deep learning models. Comput Biol Med 2021; 136: 104737.
[18] Li B, Wang P, Jiao J, Wei H, Xu W and Zhou P. Roles of the RANKL-RANK axis in immunity-implications for pathogenesis and treatment of bone metastasis. Front Immunol 2022; 13: 824117.
[19] Okamoto K. Role of RANKL in cancer development and metastasis. J Bone Miner Metab 2021; 39: 71-81.
[20] Cheng N, Liu J, Chen C, Zheng T, Li C and Huang J. Prediction of lung cancer metastasis by gene expression. Comput Biol Med 2023; 153: 106490.
[21] Guo Y, Lin Q, Zhao S, Li T, Cao Y, Man Z and Zeng X. Automated detection of lung cancer-caused metastasis by classifying scintigraphic images using convolutional neural network with residual connection and hybrid attention mechanism. Insights Imaging 2022; 13: 24.
[22] Lin Z, Wang R, Zhou Y, Wang Q, Yang CY, Hao BC and Ke CF. Prediction of distant metastasis and survival prediction of gastric cancer patients with metastasis to the liver, lung, bone, and brain: research based on the SEER database. Ann Transl Med 2022; 10: 16.
[23] Sosa MS, Bragado P and Aguirre-Ghiso JA. Mechanisms of disseminated cancer cell dormancy: an awakening field. Nat Rev Cancer 2014; 14: 611-622.
[24] Cheng N, Chen C, Li C and Huang J. Inferring Cell-type-specific genes of lung cancer based on deep learning. Curr Gene Ther 2022; 22: 439-448.
[25] Cao Z, Zheng R, Li J, Wang X, Ding C, Zhang F, Geng J, Wei Z and Fan R. Risk factors of bone metastasis in lung adenocarcinoma. BMC Pulm Med 2025; 25: 299.
[26] De Luca A, Carotenuto A, Rachiglio A, Gallo M, Maiello MR, Aldinucci D, Pinto A and Normanno N. The role of the EGFR signaling in tumor microenvironment. J Cell Physiol 2008; 214: 559-567.
[27] Taverna S, Pucci M, Giallombardo M, Di Bella MA, Santarpia M, Reclusa P, Gil-Bazo I, Rolfo C and Alessandro R. Amphiregulin contained in NSCLC-exosomes induces osteoclast differentiation through the activation of EGFR pathway. Sci Rep 2017; 7: 3170.
[28] Tanaka I, Hori K, Koyama J, Gen S, Morise M, Kodama Y, Matsui A, Miyazawa A, Hase T, Hibino Y, Yokoyama T, Kimura T, Yoshida N, Sato M and Ishii M. Femoral bone metastasis is a poor

prognostic factor in EGFR-TKIs-treated patients with EGFR-mutated non-small-cell lung cancer: a retrospective, multicenter cohort study. Ther Adv Med Oncol 2024; 16: 17588359241303090.
[29] Huang SM, Yang JJ, Chen HJ, Wu SP, Bai XY, Zhou Q, Tu HY and Wu YL. Epidermal growth factor receptor is associated with the onset of skeletal related events in non-small cell lung cancer. Oncotarget 2017; 8: 81369-81376.
[30] Teng X, Han K, Jin W, Ma L, Wei L, Min D, Chen L and Du Y. Development and validation of an early diagnosis model for bone metastasis in non-small cell lung cancer based on serological characteristics of the bone metastasis mechanism. EClinicalMedicine 2024; 72: 102617.
[31] Yu S, Jiang Z, Zhang L, Niu X, Wang L, Wu N and Ma J. Chinese expert consensus statement on clinical diagnosis and treatment of malignant tumor bone metastasis and bone related diseases. Chin Ger J Clin Oncol 2010; 9: 1-12.
[32] Gamage S, Mohamed Jiffry MZ, Sriharan P, Velayuthum S and Gunawardana T. Bony metastasis to the radius as the initial presentation of a lung adenocarcinoma. Cureus 2023; 15: e36855.
[33] Duan J, Fang W, Xu H, Wang J, Chen Y, Ding Y, Dong X, Fan Y, Gao B, Hu J, Huang Y, Huang C, Huang D, Liang W, Lin L, Liu H, Ma Z, Shi M, Song Y, Tang C, Wang J, Wang L, Wang Y, Wang Z, Yang N, Yao Y, Yu Y, Yu Q, Zhang H, Zhao J, Zhao M, Zhu Z, Niu X, Zhang L and Wang J. Chinese expert consensus on the diagnosis and treatment of bone metastasis in lung cancer (2022 edition). J Natl Cancer Cent 2023; 3: 256-265.
[34] Wang H, Wang Z, Zhang G, Zhang M, Zhang X, Li H, Zheng X and Ma Z. Driver genes as predictive indicators of brain metastasis in patients with advanced NSCLC: EGFR, ALK, and RET gene mutations. Cancer Med 2020; 9: 487-495.
[35] Yang H, Hong W, Ding J, Yuan W, Ye H, Lin T, Hu Q, Jin X, Wen L, Liu D and Lei M. Driver genes and genomic instability predict the incidence and outcome of brain metastases. Curr Cancer Drug Targets 2025; [Epub ahead of print].
[36] Schäfer S, Seiler I, Balermpas P, von Wachter C, Loi M, Greto D, Schunn AS, Drabke S, Klischies K, Wittenstein O, Willner J, Lohaus F, Kästner L, Meents J, Bank P, Slavik M, Burkon P, Partl R, Müller JA, Dzierma Y, Mader T, Trommer M, Gkika E, Rühle A, Guckenberger M, Moustakis C, Brunner T, Blanck O, Boda-Heggemann J, Nicolay NH and Nägler F. Outcome of patients with lung cancer treated with stereotactic body radiotherapy for bone oligometastases - a European multicenter cohort study. Radiat Oncol 2026; 21: 77.
[37] Hao W, Yang C, Liu W, Huang Z, Zhuang H, Lu WW and Chen Y. Metastatic lung adenocarcinoma causes extensive destruction of the hip and pelvis. Discov Oncol 2025; 17: 167.
[38] Raschka T, Weiss S, Reiter A, Barg A, Schlickewei C, Frosch KH and Priemel M. Outcomes and prognostic factors after surgery for bone metastases in the extremities and pelvis: a retrospective analysis of 140 patients. J Bone Oncol 2022; 34: 100427.
[39] Yang F, Sun K, Li F, Li X, Shi J, Sun X, Hong Y, Jiang G, Zhu Y and Song X. The prognostic impact of epidermal growth factor receptor mutation in clinical stage I lung adenocarcinoma. Ann Thorac Surg 2024; 117: 1111-1119.
[40] Kim H, Park S, Jung HA, Sun JM, Lee SH, Ahn JS and Ahn MJ. EGFR mutation-positive unresectable stage III non-squamous lung cancer is associated with a high incidence of brain metastasis. Cancer Res Treat 2023; 55: 498-505.
[41] Ying H, Kimmelman AC, Lyssiotis CA, Hua S, Chu GC, Fletcher-Sananikone E, Locasale JW, Son J, Zhang H, Coloff JL, Yan H, Wang W, Chen S, Viale A, Zheng H, Paik JH, Lim C, Guimaraes AR, Martin ES, Chang J, Hezel AF, Perry SR, Hu J, Gan B, Xiao Y, Asara JM, Weissleder R, Wang YA, Chin L, Cantley LC and DePinho RA. Oncogenic Kras maintains pancreatic tumors through regulation of anabolic glucose metabolism. Cell 2012; 149: 656-670.
[42] Brouns AJWM, Hendriks LEL, Robbesom-van den Berge IJ, Driessen AJHM, Roemen GMJM, van Herpen BLJ, Dekkers Z, Heitzer B, Leunissen DJG, Moonen L, Lunde R, Westenend M, van Driel M, Speel EM and Dingemans AC. Association of RANKL and EGFR gene expression with bone metastases in patients with metastatic non-small cell lung cancer. Front Oncol 2023; 13: 1145001.
[43] Yi T, Lee HL, Cha JH, Ko SI, Kim HJ, Shin HI, Woo KM, Ryoo HM, Kim GS and Baek JH. Epidermal growth factor receptor regulates osteoclast differentiation and survival through cross-talking with RANK signaling. J Cell Physiol 2008; 217: 409-422.
[44] Hsu PC, Lee SH, Chiu LC, Lee CS, Wu CE, Kuo SC, Ju JS, Huang AC, Li SH, Ko HW, Yang CT and Wang CC. Afatinib in Untreated Stage IIIB/IV lung adenocarcinoma with major uncommon epidermal growth factor receptor (EGFR) mutations (G719X/L861Q/S768I): a multicenter observational study in Taiwan. Target Oncol 2023; 18: 195-207.
[45] Knapp B, Flanagan M, Grandhi N, Ganesh B, Cittolin Santos G, Gao F, Samson P, Govindan R and Morgensztern D. The incidence and risk factors predictive of bone metastases at initial

diagnosis of malignancy. J Clin Oncol 2023; 41: e18816.

[46] Day KC, Lorenzatti Hiles G, Kozminsky M, Dawsey SJ, Paul A, Broses LJ, Shah R, Kunja LP, Hall C, Palanisamy N, Daignault-Newton S, El-Sawy L, Wilson SJ, Chou A, Ignatoski KW, Keller E, Thomas D, Nagrath S, Morgan T and Day ML. HER2 and EGFR overexpression support metastatic progression of prostate cancer to bone. Cancer Res 2017; 77: 74-85.

[47] Loeffler E, Ancel J, Dalstein V, Deslée G, Polette M and Nawrocki-Raby B. HER2 alterations in non-small cell lung cancer: biologico-clinical consequences and interest in therapeutic strategies. Life (Basel) 2023; 14: 64.

Supplementary Table 1. Spatio-temporal feature of BM in lung cancer with different driver gene types

	Driverless N (%)	ALK N (%)	Other Gene N (%)	KRAS N (%)	EGFR N (%)	HER2 N (%)	χ^2	*P*
Spatial Feature								
Cranial	3 (5.2)	3 (21.4)	3 (10.3)	4 (12.5)	36 (17.6)	2 (12.5)	6.821	0.186
Non-Cranial	55 (94.8)	11 (78.6)	26 (89.7)	28 (87.5)	168 (82.4)	14 (87.5)		
Spinal	41 (70.7)	11 (78.6)	18 (62.1)	21 (65.6)	144 (70.6)	14 (87.5)	4.023	0.546
Non-Spinal	17 (29.3)	3 (21.4)	11 (37.9)	11 (34.4)	60 (29.4)	2 (12.5)		
Pelvic	16 (27.6)	7 (50.0)	11 (37.9)	15 (46.9)	118 (57.8)	12 (75.0)	22.423	< 0.001*
Non-Pelvic	42 (72.4)	7 (50.0)	18 (62.1)	17 (53.1)	86 (42.2)	4 (25.0)		
Extremity Bones	17 (29.3)	4 (28.6)	6 (20.7)	10 (31.3)	72 (35.3)	4 (25.0)	3.359	0.645
Non-Extremity Bones	41 (70.7)	10 (71.4)	23 (79.3)	22 (68.8)	132 (64.7)	12 (75.0)		
Thoracic Bone	30 (51.7)	7 (50.0)	19 (65.5)	21 (65.6)	131 (64.2)	7 (43.8)	6.228	0.285
N-Thoracic Bone	28 (48.3)	7 (50.0)	10 (34.5)	11 (34.4)	73 (35.8)	9 (56.3)		
Temporal Feature								
Simultaneous BM	39 (67.2)	9 (64.3)	23 (79.3)	29 (90.6)	174 (85.3)	15 (93.8)	16.192	0.006*
N-Simultaneous BM	19 (32.8)	5 (35.7)	6 (20.7)	3 (9.4)	30 (14.7)	1 (6.2)		
Spatio-temporal Feature								
Simultaneous Cranial BM								
Yes	2 (3.4)	3 (21.4)	3 (10.3)	4 (12.5)	34 (16.5)	2 (12.5)	7.762	0.101
No	56 (96.4)	11 (78.6)	26 (89.7)	28 (87.5)	170 (83.5)	14 (87.5)		
Simultaneous Spinal BM								
Yes	28 (48.3)	7 (50.0)	16 (55.2)	20 (62.5)	123 (59.7)	13 (81.3)	6.943	0.225
No	30 (51.7)	7 (50.0)	13 (44.8)	12 (37.5)	81 (40.3)	3 (18.7)		
Simultaneous Pelvic BM								
Yes	12 (20.7)	5 (35.7)	11 (37.9)	15 (46.9)	102 (50.0)	12 (75.0)	22.859	< 0.001*
No	46 (79.3)	9 (64.3)	18 (62.1)	17 (53.1)	102 (50.0)	4 (25.0)		
Simultaneous Extremity BM								
Yes	12 (20.7)	2 (14.3)	4 (13.8)	9 (28.1)	65 (31.6)	4 (25.0)	7.347	0.196
No	46 (79.3)	12 (85.7)	25 (86.2)	23 (71.9)	139 (68.4)	12 (75.0)		
Simultaneous Thoracic BM								
Yes	25 (43.1)	6 (42.9)	15 (51.7)	19 (59.4)	116 (56.3)	7 (43.8)	5.165	0.396
No	33 (56.9)	8 (57.1)	14 (48.3)	13 (40.6)	88 (43.7)	9 (56.2)		

Note: *There is a statistically significant difference.

Supplementary Table 2. Spatio-temporal Feature of BM in lung cancer with different EGFR genotypes

	EGFR 19 N (%)	EGFR 21 N (%)	Other EGFR N (%)	Co-mutation N (%)	χ^2	*P*
Spatial Feature						
Cranial	18 (22.0)	12 (14.8)	4 (19.0)	2 (10.0)	2.325	0.552
Non-Cranial	64 (78.0)	69 (85.2)	17 (81.0)	18 (90.0)		
Spinal	66 (80.5)	49 (60.5)	14 (66.7)	15 (75.0)	8.189	0.042
Non-Spinal	16 (19.5)	32 (39.5)	7 (33.3)	5 (25.0)		
Pelvic	52 (63.4)	42 (51.9)	13 (61.9)	11 (55.0)	2.445	0.485
Non-Pelvic	30 (36.6)	39 (48.1)	8 (38.1)	9 (45.0)		
Extremity Bone	35 (42.7)	21 (25.9)	10 (47.6)	6 (30.0)	6.715	0.082
Non-Extremity Bone	47 (57.3)	60 (74.1)	11 (52.4)	14 (70.0)		
Thoracic Bone	55 (67.1)	51 (63.0)	14 (66.7)	11 (55.0)	1.141	0.767
N-Thoracic Bone	27 (32.9)	30 (37.0)	7 (33.3)	9 (45.0)		
Temporal Feature						
Simultaneous BM	71 (86.6)	72 (88.9)	16 (76.2)	15 (75.0)	4.021	0.236
N-Simultaneous BM	11 (13.4)	9 (11.1)	5 (23.8)	5 (25.0)		
Spatio-temporal Feature						
Simultaneous Cranial BM						
Yes	17 (20.7)	11 (13.6)	4 (19.0)	2 (10.0)	2.257	0.557
No	65 (79.3)	70 (96.4)	17 (81.0)	18 (90.0)		
Simultaneous Spinal BM						
Yes	59 (72.0)	44 (54.3)	9 (42.9)	11 (55.0)	8.763	0.033
No	23 (28.0)	37 (45.7)	12 (57.1)	9 (45.0)		
Simultaneous Pelvic BM						
Yes	45 (54.9)	38 (46.9)	11 (52.4)	8 (40.0)	1.874	0.599
No	37 (45.1)	43 (53.1)	10 (47.6)	12 (60.0)		
Simultaneous Extremity BM						
Yes	31 (37.8)	19 (23.5)	9 (42.9)	6 (30.0)	5.171	0.160
No	51 (62.2)	62 (76.5)	12 (57.1)	14 (70.0)		
Simultaneous Thoracic BM						
Yes	50 (61.0)	45 (55.6)	13 (61.9)	8 (40.0)	0.613	0.893
No	32 (39.0)	36 (44.4)	8 (38.1)	12 (60.0)		

Supplementary Table 3. Summary descriptives table by groups

Factors	Training Group N = 247 (%)	Validation Group N = 106 (%)	*P*
Age			0.423
< 60	95 (38.5)	36 (34.0)	
≥ 60	152 (61.5)	70 (66.0)	
Gender			0.790
Male	129 (52.2)	57 (53.8)	
Female	118 (47.8)	49 (46.2)	
Smoking history			0.955
Never	158 (64.0)	67 (63.2)	
Past	57 (23.1)	24 (22.6)	
Current	32 (13.0)	15 (14.2)	
ECOG			0.394
0-2	138 (55.9)	54 (50.9)	
> 2	109 (44.1)	52 (49.1)	
ALP (U/L)			0.155
≤ 150	188 (76.1)	73 (68.9)	
> 150	59 (23.9)	33 (31.1)	
LDH (U/L)			0.710
≤ 250	152 (61.5)	63 (59.4)	
> 250	95 (38.5)	43 (40.6)	
Ca^{2+} (mmol/L)			0.903
≤ 2.52	237 (96.0)	102 (96.2)	
> 2.52	10 (4.0)	4 (3.8)	
ProGRP (pg/ml)			0.960
≤ 69.2	194 (78.5)	83 (78.3)	
> 69.2	53 (21.5)	23 (21.7)	
SCC (ng/L)			0.996
≤ 2.7	212 (85.8)	91 (85.8)	
> 2.7	35 (14.2)	15 (14.2)	
CEA (ng/L)			0.882
≤ 5	53 (21.5)	22 (20.8)	
> 5	194 (78.5)	84 (79.2)	
CYFRA21-1 (ng/L)			0.457
≤ 3.3	43 (17.4)	22 (20.8)	
> 3.3	204 (82.6)	84 (79.2)	
NSE (ng/L)			0.324
≤ 16.5	100 (40.5)	37 (34.9)	
> 16.5	147 (59.5)	69 (65.1)	
SII			0.684
≤ 609.9	67 (27.1)	31 (29.2)	
> 609.9	180 (72.9)	75 (70.8)	
PNI			0.767
≤ 45.75	95 (38.5)	39 (36.8)	
> 45.75	152 (61.5)	67 (63.2)	
D-dimer (mg/L)			0.729
< 0.243	91 (36.8)	37 (34.9)	
≥ 0.243	156 (63.2)	69 (65.1)	

Pathological type			0.565
Squamous Cell Carcinoma	14 (5.7)	7 (6.6)	
Adenocarcinoma	223 (90.3)	97 (91.5)	
Other type	10 (4.0)	2 (1.9)	
T stage			0.898
T1-T2	95 (38.5)	40 (37.7)	
T3-T4	152 (61.5)	66 (62.3)	
N stage			0.445
N0-N1	63 (25.5)	23 (21.7)	
N2-N3	184 (74.5)	83 (78.3)	
Number of lung cancer lesions			0.575
Single	189 (76.5)	84 (79.2)	
Multiple	58 (23.5)	22 (20.8)	
Regional lymph node metastasis			0.889
Yes	34 (13.8)	14 (13.2)	
No	213 (86.2)	92 (86.8)	
Distant lymph node metastasis			0.917
Yes	118 (47.8)	50 (47.2)	
No	129 (52.2)	56 (52.8)	
Distant metastasis			0.457
Yes	204 (82.6)	84 (79.2)	
No	43 (17.4)	22 (20.8)	
Driver gene type			0.725
Driverless Mutation	44 (17.8)	14 (13.2)	
ALK+	10 (4.0)	4 (3.8)	
Other Driver Genes	21 (8.5)	8 (7.5)	
KRAS+	21 (8.5)	11 (10.4)	
EGFR+	138 (55.9)	66 (62.3)	
HER2+	13 (5.3)	3 (2.8)	
Number of Bone Metastasis			0.233
Single	61 (24.7)	20 (18.9)	
Multiple	186 (75.3)	86 (81.1)	
Cranial Metastasis			0.375
No	216 (87.4)	89 (84.0)	
Yes	31 (12.6)	17 (16.0)	
Spinal Metastasis			0.183
No	110 (44.5)	36 (34.0)	
Yes	137 (55.5)	70 (66.0)	
Limbs Extremities			0.631
No	182 (73.7)	75 (70.8)	
Yes	65 (26.3)	31 (29.2)	
Thoracic Metastasis			0.562
No	122 (49.4)	43 (40.6)	
Yes	125 (50.6)	63 (59.4)	

Supplementary Table 4. Ailed scoring criteria for the nomogram model of simultaneous pelvic metastasis

Factors	Category	Points
ProGRP (pg/ml)	≤ 69.2 (0)	0
	> 69.2 (1)	31
Spinal Metastasis	No (0)	0
	Yes (1)	28
Limbs Extremities	No (0)	0
	Yes (1)	39
Number of Bone Metastasis	Single (0)	0
	Multiple (1)	42
Driver gene type	Driverless Mutation (0)	0
	ALK+ (1)	29
	Other Driver Genes (2)	33
	KRAS+ (3)	34
	EGFR+ (4)	41
	HER2+ (5)	100

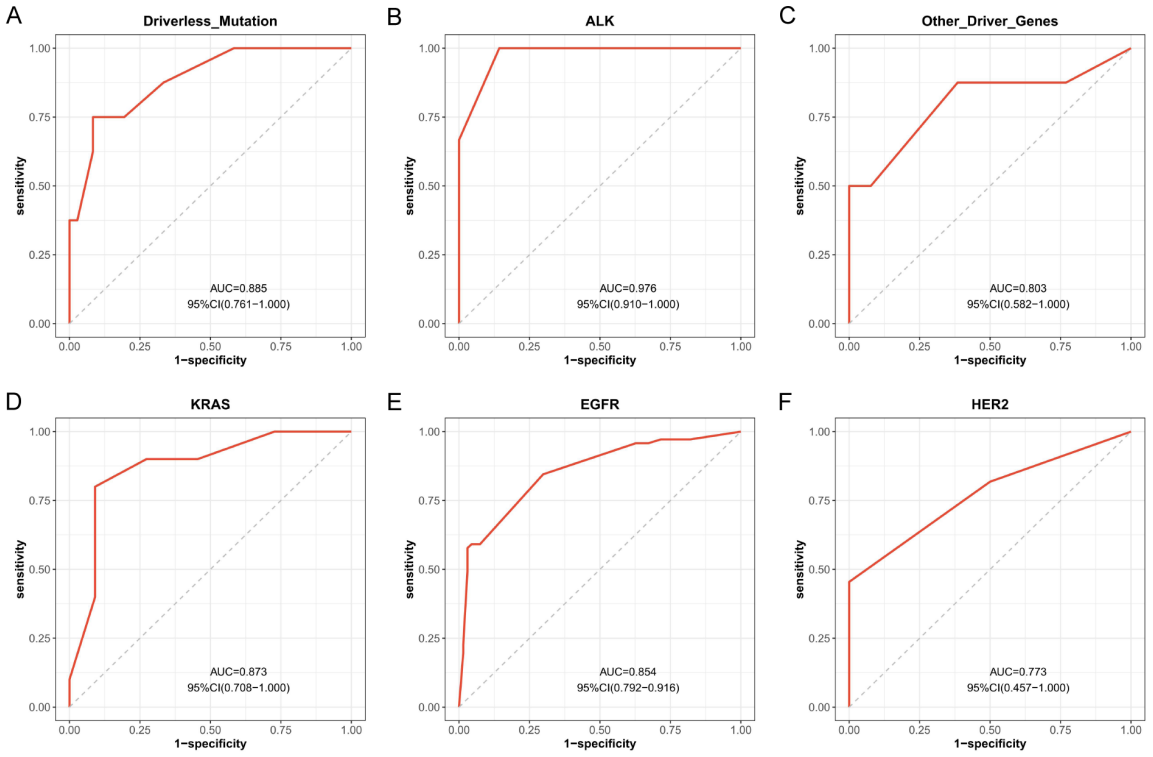

Supplementary Figure 1. The ROC curves for Subgroup analyses of Different Driver Gene. ROC: Receiver Operating Characteristic curve; AUC: Area under the Receiver Operating Characteristic curve.